Journal of The Electrochemical Society, **159** (5) K136-K140 (2012)
0013-4651/2012/159(5)/K136/5/$28.00 © The Electrochemical Society

The Differences in Optical Characteristics of TiO_2 and TiO_2/AAO Nanotube Arrays Fabricated by Atomic Layer Deposition

Yung-Huang Chang,[a] Chien-Min Liu,[a] Chih Chen,[a,z] Hsyi-En Cheng,[b] and Tien-Chang Lu[c]

[a]*Department of Materials Science and Engineering and* [c]*Department of Photonics, National Chiao Tung University, Hsin-chu 30010, Taiwan*
[b]*Department of Electro-Optical Engineering, Southern Taiwan University, Tainan 710, Taiwan*

Self-aligned TiO_2 nanotube arrays can be fabricated by atomic layer deposition (ALD) and anodic oxide template (AAO) on Si or quartz substrates. In this study, we compare the hetero-junction effects on optical characteristics of TiO_2 nanotube arrays for the cases with AAO stayed intact and after AAO was etched away selectively. Due to the space confinement effect that can occur only in the TiO_2/AAO nanotubes, the photoluminance intensity of TiO_2 material is enhanced about 5 times for TiO_2/AAO nanotubes compared with the TiO_2 nanotubes. On the contrary, under 0 V bias, quantum efficiency of the TiO_2/AAO nanotubes is 5.8 times lower than the TiO_2 nanotubes because of higher probability for the recombination of photon-generated electron-hole pairs from the space confinement effect in TiO_2/AAO nanotube arrays. When the bias reached 1 V, the TiO_2 nanotubes still revealed more outstanding photon-to-electron transformation properties than the TiO_2/AAO nanotubes. However, the quantum efficiency of TiO_2/AAO nanotubes began to exceed TiO_2 nanotubes when the bias is over 2 V. This phenomenon could result from the restraint of the recombination of photo-generated electron-hole pairs under high field strength and the increase in an amount of photo-generated carriers injected from AAO template.
 [DOI: 10.1149/2.045205jes]

Manuscript submitted October 28, 2011; revised manuscript received February 1, 2012. Published February 29, 2012.

In recent years, TiO_2 material has attracted a lot of interests due to its particular optoelectronic characteristics, which make it a very promising candidate in green energy. Because of its excellent optical properties, TiO_2 has been utilized in many applications, such as photoelectrochemical water splitting,[1,2] photoelectrochemical generation of hydrogen,[3] dye sensitized solar cells[4,5] and photocatalysis,[6,7] etc. In 1972, Fujishima and Honda[8] reported that water can be decomposed directly when TiO_2 plate placed in water was irradiated with wavelengths shorter than 190 nm. In 1991, M. Grätzel et al.[4] fabricated the dye sensitized solar cells (DSSCs) using nanocrystalline porous TiO_2 as electrode to convert solar light to electron-hole pairs. Furthermore, in order to enhance the optical application limited by the innate bandgap (3.2 eV), TiO_2 doped with N,[9] C[10] and S[11] have been studied as well. Several factors can affect the photoconductive characteristics, including crystallization, nanostructure, film thickness, post treatment of annealing and contact with metal. So far, most of the research efforts have been emphasizing on modifying material properties in the hope of enhancing its absorbability to extend from UV region to visible region.[9–12] However, it should be noted that in the study of traditional semiconductor, hetero-junction was heavily emphasized because it determines a device's ultimate performance. In addition, the hetero-junction effects are magnified in a device's landscape and become more critical especially for nanoscale materials. Therefore, besides concentrating efforts on modification of intrinsic material, hetero-junction studies of devices or sensors under UV light illumination should not be neglected. However, the studies in this field are scarce, especially in nanostructure systems.

The synthesis methods of TiO_2 nanotubes includes anodic oxidation,[13–15] hydrothermal synthesis[16–18] and template method.[19–22] Among these growth methods, the utilization of atomic layer deposition (ALD) technology with the application of anodic-oxide-template (AAO)[19,23,24] template provides well-controlled method to prepare vertically aligned TiO_2 nanotube arrays. In this study, we investigate the photoresponse of TiO_2 with AAO stayed intact and after AAO was etched away selectively. The hetero-junction effects on the photoconductive characteristics of TiO_2 only nanotubes and TiO_2/AAO nanotubes under ultraviolet illumination in the air environment were investigated, and the mechanism of the carrier transportation was discussed using energy band diagram.

Experimental

An AAO layer was first fabricated onto P-type (100) silicon or quartz substrates as a template layer with methods presented in previous study.[25] The Si or quartz substrate was then placed in a quartz tube reactor maintained at 1.6×10^{-1} Torr and 400°C. The precursors of $TiCl_4$ and H_2O, kept separately in a canister at 30 ± 1°C and 25 ± 1°C, were used as Ti and O source, respectively. Pure Ar gas (99.999 %) was used as carrier gas and purge gas. Each deposition cycle was consisted of eight steps, which included $TiCl_4$ reactant, pump-down, Ar purge, pump-down, H_2O reactant, pump-down, Ar purge, and pump-down. Typical pulse times for $TiCl_4$ and H_2O precursors were 1s, and the purge time was 1s. In order to remove the residual reactants and by-products efficiently, the 1s pump-down step was added after each step. To prepare TiO_2 nanotube arrays, 200-cycle deposition parameter was introduced. After the deposition, TiO_2 was deposited on side walls and top surface of the AAO template layer. The TiO_2 film on the top surface of the AAO was then removed with mechanical polishing. Finally, for the case without AAO, the AAO template was selectively removed by a 0.1 wt% sodium hydroxide (NaOH(aq)) solution, and TiO_2 nanotube arrays can be fabricated on the Si substrate or quart substrate.

An ITO film (450 nm) and an Al film was used as electrode and back electrode for ohmic contact, and were deposited on the top of TiO_2 and TiO_2/AAO nanotube arrays using e-gun evaporation system and thermal evaporation coater, respectively as shown in Fig. 1. UV-vis spectrometer (U-3500, Hitachi) was utilized to measure the continued light absorption characteristics of TiO_2 nanotube arrays and AAO template on quartz substrates. Photoluminescence (PL) of an AAO template, AAO/TiO_2 nanotube arrays and TiO_2 only nanotube arrays on silicon substrates were recorded using a He-Cd laser of 325 nm wavelength as the excitation source at room temperature. The current characteristics of specimens were recorded using a keithley 2400 sourcemeter. Due to the measuring requirement, a small voltage of $\sim 10^{-6}$ V is applied automatically by the keithley 2400 sourcemeter when the equipment is set up to 0 V bias. Furthermore, it is regarded as short circuit ($\sim$0 V) since 10^{-6} V can be considered negligible. The photoresponse study was performed under UV illumination of ~ 21 mW/cm^2 ($\lambda = 365$ nm) in the air at room temperature. Figure 1 shows the schematic drawing of the setup for the measurement of the shot circuit current. UV light was shone on the sample through the ITO electrode. The ITO layer was connected to the anode of the sourcemeter and the Al electrode was attached to the cathode of the sourcemeter. Field-emission scanning electron microscope

[z] E-mail: chih@mail.nctu.edu.tw

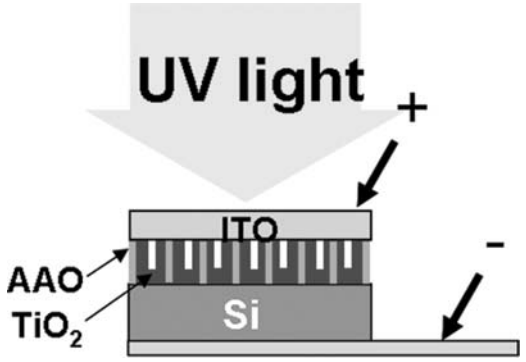

Figure 1. Schematic diagram showing the experimental setup for photoresponse measurement.

(FESEM, JSM-6500F) and transmission electron microscope (TEM) were utilized to examine the morphology of the nanotube arrays.

Results and Discussion

With the aid of the ALD and AAO template, self-aligned regular arrays of TiO_2 nanotube can be fabricated. Figures 2a and 2b show the cross-sectional SEM images of TiO_2/AAO and TiO_2 nanotube arrays with ITO electrode on the top, respectively. No residual AAO template was observed in Fig. 2b and the height of TiO_2 nanotube array is about 600 nm. In particular, the tubular structure of TiO_2 nanotube arrays can be seen clearly in Fig. 2b. The nanotubes are vertical to the Si substrate, and have a good contact with the ITO electrode. Figure 2c show the plan-view TEM image of the TiO_2 nanotube arrays in the AAO pores. The average diameter of the nanotube is about 75 nm and the wall thickness is about 8.8 nm. As shown in Fig. 2c, the gap between the neighboring TiO_2 nanotubes is approximately 60 nm. Therefore the aspect ratio of the gap is as large as 10. Therefore, the sputtered ITO film cannot fill the gap between the neighboring TiO_2 nanotubes, as shown in Figure 2b.

To provide the reference of the optical characteristics, the absorbance measurements were performed for the AAO template layer and the TiO_2 nanotube arrays fabricated on quartz substrates. Figures 3a and 3b show the absorbance spectra of an AAO template and TiO_2 nanotube arrays on quartz substrates. When the wavelength of incident light is 325 nm, the absorbance of AAO is 0.091 and the absorbance of TiO_2 nanotube arrays is 1.6. The absorbability of TiO_2 is 17.6 times that of the AAO template. With the incident wavelength of 365 nm, the absorbance of AAO and TiO_2 is 0.096 and 0.16, respectively. The absorbability of TiO_2 nanotube arrays is 1.66 times that of AAO template. Therefore, TiO_2 nanotube arrays play a more important role in UV absorption in the wavelength 325 or 365 nm than the AAO template.

Photoluminance was carried out to further characterize the optical properties of the TiO_2 nanotube arrays. Figure 4a shows the PL spectra of TiO_2/AAO nanotube arrays, TiO_2 nanotube arrays and the AAO template on Si substrates. AAO has a bandgap of 6.2 eV.[26] Theoretically, a light source with the wavelength of 325 nm is not sufficient to provide energy for electrons excited from the valance band to conduction band. However, it is known that the surface of AAO template is primarily amorphous aluminum oxide,[27] and the surface defects may provide alternate paths for electron transition. Therefore, AAO template can absorb incident light source of 325 nm wavelength. As shown in Figure 4a, AAO template has the highest PL intensity, followed by TiO_2/AAO, and then TiO_2 nanotubes. Even though TiO_2 shows better light absorbance than AAO, the weaker PL emission as compared to AAO could be due to the following two reasons. First, TiO_2 has an indirect bandgap that prevents efficient radiative recombination. Second, the high percentage of amorphous Al_2O_{3-x} on the AAO template provides oxygen vacancy levels for better optical transitions.[26] To

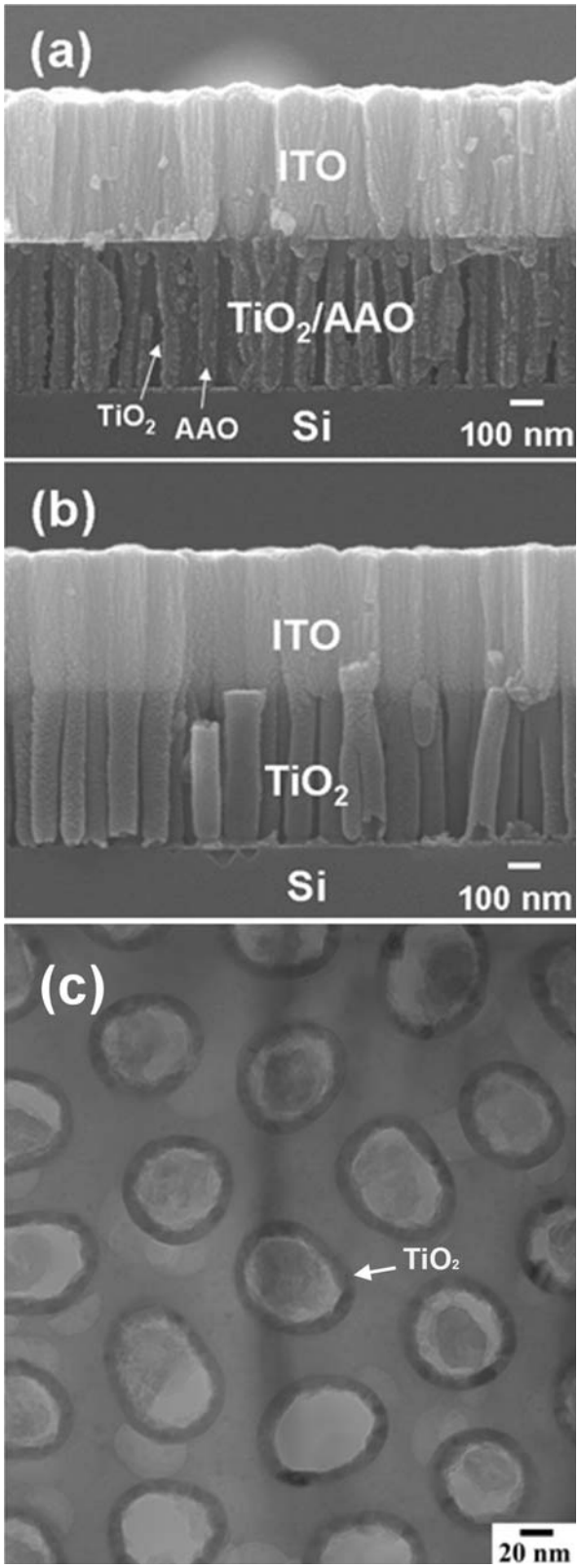

Figure 2. Cross-sectional SEM images of TiO_2 nanotube arrays after 200 cycles at 400°C: (a) TiO_2 nanotube arrays. AAO template was etched away selectively; (b) TiO_2/AAO nanotube arrays. The TiO_2 nanotubes are surrounded by AAO. (c) Plan-view TEM image of the TiO_2 nanotube arrays after 200 cycles at 400°C.

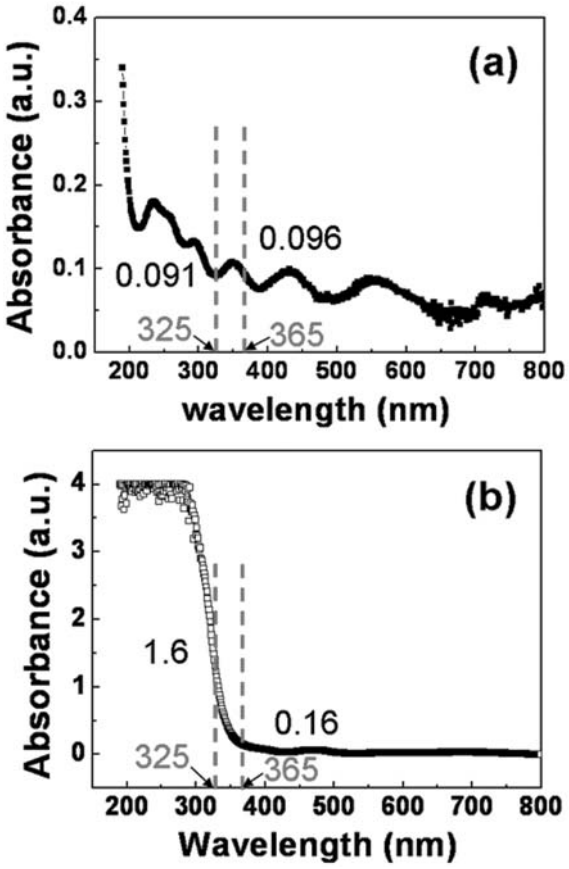

Figure 3. Absorption spectra of (a) the AAO template; and (b) the TiO_2 nanotube arrays on quartz substrates.

further investigate the reason why TiO_2/AAO nanotubes have better PL emission than TiO_2 nanotubes, we use Gauss fitting to analyze the sub component of the PL spectra. The PL spectrum of the AAO template is known to consist of two sub-bands: 410 nm and 475 nm,[28,29] as shown in Figure 4b. TiO_2/AAO has 5 sub-bands and they are 386 nm, 410 nm, 465 nm, 475 nm and 525 nm as shown in Figure 4c. TiO_2 nanotubes have only one band at 525 nm,[30–33] as shown in Figure 4d. The 410 nm and 475 nm sub-bands belong to the AAO template.[28,29] According to the literatures, the visible sub-bands located at 464 nm and 525 nm are resulted from the emission caused by oxygen vacancies, including the F center and F^+ center, respectively. The F center is the neutral oxygen vacancy at ~2.67 eV above the valence band, whereas the F^+ center is the oxygen vacancy losing one electrons at ~2.36 eV above the valence band.[30–33] Compared to the AAO template, the intensity of PL contributed from the AAO in TiO_2/AAO nanotube arrays was somewhat lower. When TiO_2 nanotubes were deposited, oxygen vacancies on the AAO surface was filled and the upper surface of AAO was covered by TiO_2, thus reducing the PL intensity.[32] On the contrary, the PL intensity attributed from TiO_2 in TiO_2/AAO nanotube arrays was higher compared to TiO_2 only nanotube arrays. The phenomenon can be attributed to the space confinement effect in TiO_2/AAO nanotubes. In the TiO_2/AAO nanotubes case, the photogenerated electrons were swept from the depletion region into TiO_2 due to the potential gradient. The enhanced numbers of carriers were therefore confined in the narrow TiO_2 wall, which could enhance the PL intensity.[34] As a result, the contribution of PL from TiO_2 in TiO_2/AAO nanotube arrays was 5 times that of TiO_2 only nanotube arrays. The sub-band of 386 nm can be contributed from either TiO_2[30,31] or AAO.[35] Further investigation at low temperatures is needed to determine the origin of these sub-bands.

TheTiO_2/AAO and TiO_2 nanotube arrays demonstrate different Photoresponse behaviors. The short circuit current for the TiO_2/AAO nanotubes, TiO_2 nanotubes and AAO template can be obtained under UV on/off illumination cycle when the positive electrode is connected to the ITO. The measured quantum efficiencies (QE) vs. time are shown in Figure 5. The quantum efficiency,η, is expressed as

$$\eta = \frac{\text{the number of generated and collected electron} - \text{hole pairs}}{\text{the number of incident photons}}$$

$$= \frac{I_{ph}/e}{P_0/h\nu} = \frac{hc}{\lambda e}\frac{I_{ph}}{P_0}$$

where P_0 is the energy of incident UV light, h is Planck's constant, e is the charge of an electron, ν is the frequency of incident UV light, λ is the wavelength of incident UV light and c is the velocity of light,

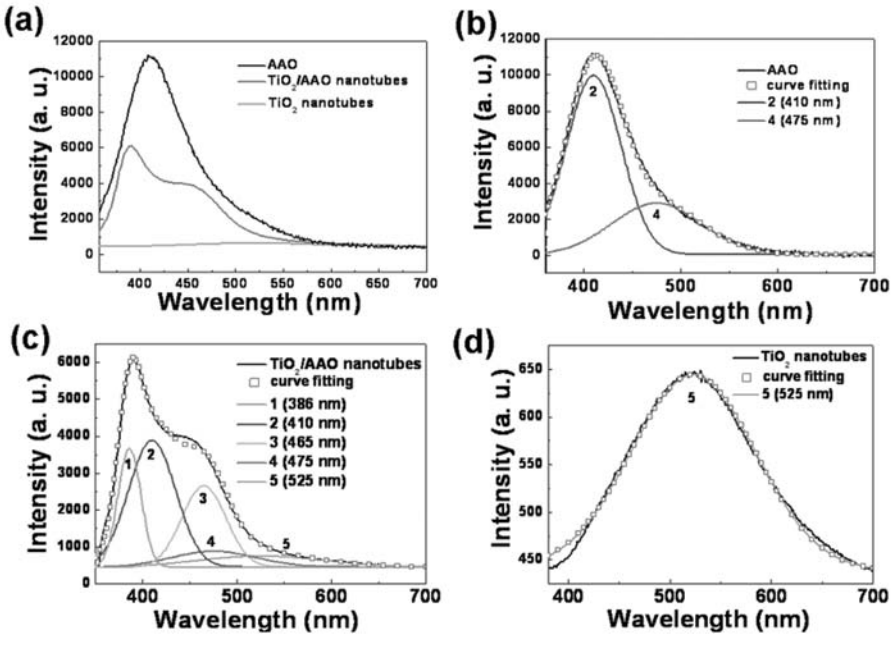

Figure 4. Photoluminance spectra of (a) the TiO_2/AAO nanotube arrays, TiO_2 nanotube arrays and AAO template. Photoluminance spectra with Gauss fitting of the (b) AAO template; (c) TiO_2/AAO nanotube arrays; and (d) TiO_2 nanotube arrays.

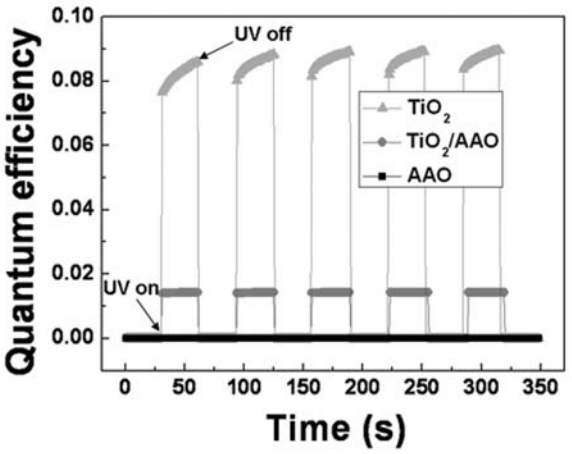

Figure 5. Quantum efficiency of the TiO_2/AAO nanotube arrays, TiO_2 nanotube arrays and AAO template at 0 V bias under on/off UV illumination cycle.

I_{ph} is the net photocurrent, which is the subtraction of the photocurrent from the leakage current. The AAO template appeared irresponsive to UV illumination. However, TiO_2/AAO or TiO_2 nanotube arrays show a steady cycle with less than 1 sec of photoresponse time.[36–38] This special characteristic is the main reason that TiO_2/AAO nanotubes and TiO_2 can be used as UV detectors. Under UV illumination, the QE obtained for TiO_2/AAO nanotubes and TiO_2 nanotubes was 0.014 and 0.082, respectively. The conversion efficiency of TiO_2 nanotube arrays is 5.86 times higher than TiO_2/AAO nanotube arrays. Due to the effect of space confinement, TiO_2 in TiO_2/AAO nanotube arrays has higher probability for the recombination of photo-generated electron-hole pairs resulting in better PL performance. However, it also means less electrons and holes remained in the conduction band and the valence band, resulting in lower QE. On the contrary, TiO_2 nanotube arrays have lower probability for the recombination of electron-hole pairs, but it also means more electron and holes are remained in the conduction and the valence band. As a result, TiO_2 has higher QE but lower PL.

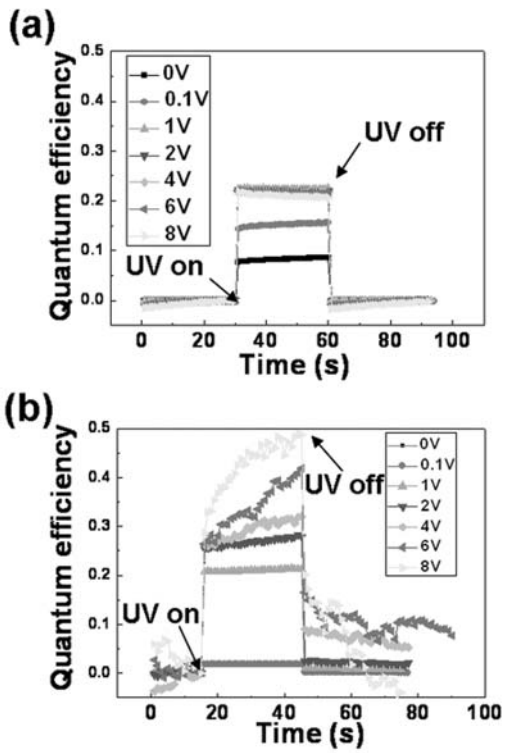

Figure 6. Measured quantum efficiency of (a) TiO_2 nanotube arrays; and (b) TiO_2/AAO nanotube arrays under on/off UV illumination at different biases.

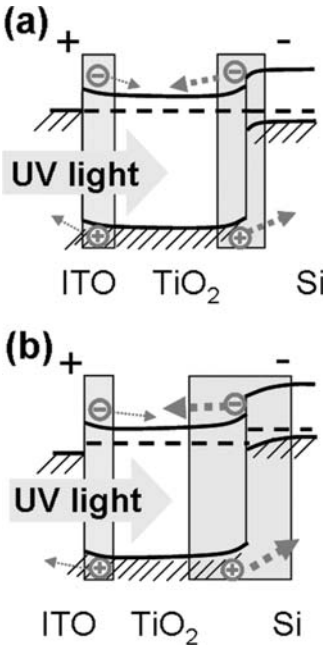

Figure 7. Energy band diagram of the ITO/TiO_2/Si diode: (a) Under 0 V bias; and (b) when positive bias is applied to the ITO electrode.

Figure 6 presents the QE results of TiO_2 nanotubes and TiO_2/AAO nanotubes under on/off illumination cycle at different biases. The overall diode characteristics of ITO/TiO_2/Si structures are determined by the variation of depletion width of ITO/TiO_2 and TiO_2/Si heterojunctions. When a reverse bias is applied, the TiO_2/Si heterojunction governs the photo-to-current conversion efficiency. As shown schematically in Figure 7, the area of depletion region increases with a larger reverse bias, and so is the number of electron-hole pairs, as discussed in detail in previous study.[39] Therefore, when the bias was increased from 0, 0.1 V to 1 V, QE of TiO_2 was increased from 0.082, 0.152 to 0.224, respectively. Similar trend was also observed in TiO_2/AAO nanotube arrays, QE was increased from 0.014, 0.018 to 0.210 for bias of 0, 0.1 and 1 V, respectively. As previously mentioned, TiO_2/AAO nanotube arrays have higher recombination effect, thus resulting in lower photo-to-current conversion performance. However, as the maximum current due to the space charge limited effect is reached,[40,41] QE of TiO_2 does not further increase with increasing bias beyond 2 V as shown in Figure 6a. On the contrary, when the bias is larger than 2 V, QE for TiO_2/AAO is 0.268, higher than QE obtained for TiO_2, as shown in Figures 6a and 6b. The phenomenon may be attributed to the following two effects. First, larger bias means TiO_2/AAO is under higher electric field. High electric field such as 4.12 MV/m at 2 V increases the transportation speed of photo-generated carriers and thus restrains the recombination of electron-hole pairs resulting from the space confinement effect. Second, there are additional electrons generated from the depletion region of AAO and are transported into TiO_2 due to the potential gradient. Higher number of carriers reflects on higher QE under high electric field for TiO_2/AAO nanotubes as shown in Figure 8. Figure 8 shows the proposed energy band diagram across the TiO_2/AAO junction. When the bias is further increased to 8 V, the increasing rate of QE gradually slowed down and delayed recovery was observed, as shown in Figure 6b. This phenomenon was not observed in TiO_2. Therefore, it may be resulted from the escape of trapping photo-carriers caught by the defects at the interface of TiO_2/AAO,[42,43] and with the increase of biases, trapping

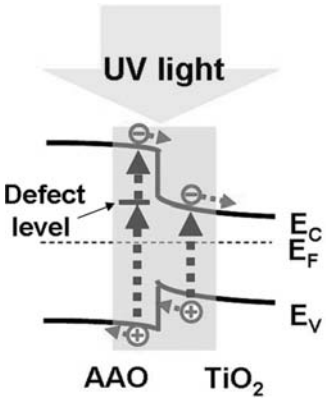

Figure 8. Proposed energy band diagram of TiO_2/AAO nanotube arrays. Under UV illumination, photo-generated carriers are transported from the depletion region to TiO_2 due to the potential gradient across the nanojunction of TiO_2/AAO.

photo-carriers were discharged more easily in a short period under UV on/off illumination cycle.

Conclusions

In summary, we studied the hetero-junction effects on optical characteristics of TiO_2 nanotube arrays fabricated by ALD and AAO on Si and quartz substrate. Due to the space confinement effect in TiO_2/AAO nanotube arrays, high probability of recombination for electron-hole pairs improves the PL intensity of TiO_2 by 5 times for TiO_2/AAO nanotubes, compared with TiO_2 nanotubes alone. At 0 V bias, however, the space confinement effect also reduced the amount of the photo-generated electron-hole pairs remained in the conduction band and the valence band; TiO_2 nanotubes therefore exhibits better QE, in the present case, 5.8 times that of TiO_2/AAO nanotube arrays. When the bias was increased to 1 V, the TiO_2 nanotubes still revealed better photon-to-electron transformation properties than TiO_2/AAO nanotubes due to the space confinement effect. However, when the bias was increased to 2 V, the high field strength would restrain the recombination phenomenon and thus increase the amount of photo-generated carriers in TiO_2 material. Furthermore, due to the injected behavior of photogenerated electron from the depletion region of AAO template into TiO_2 material, the number of carriers in TiO_2 was enhanced further. Therefore, the quantum efficiency is improved for TiO_2/AAO nanotube arrays when the biases are beyond 2 V. For the nano-scale framework, we were successful at utilizing classical knowledge of energy band diagram to explain the photo-carriers transportation under UV on/off illumination.

Acknowledgments

The authors thank the National Science Council of the Republic of China, Taiwan, for the financial support in this research under Contract No. NSC-98-2221-E-009-036-MY3.

References

1. G. K. Mor, K. Shankar, M. Paulose, O. K. Varghese, and C. A. Grimes, *Nano Lett.*, **5**, 191 (2005).
2. J. H. Park, O. O. Park, and S. Kim, *Appl. Phys. Lett.*, **89**, 163106 (2006).
3. N. N. Rao and S. Dube, *Int. J. Hydrogen energy*, **21**, 95 (1996).
4. B. O'Regan and M. Grätzel, *Nature*, **353**, 737 (1991).
5. Michael Grätze, *Nature*, **414**, 338 (2001).
6. S. P. Albu, A. Ghicov, J. M. Macak, R. Hahn, and P. Schmuki, *Nano Lett.*, **7**, 1286 (2007).
7. A. L. Linsebigler, G. Lu, and J. T. Yates, Jr., *Chem. Rev.*, **95**, 735 (1995).
8. A. Fujishima and K. Honda, *Nature*, **238**, 37 (1972).
9. A. Ghicov, J. M. Macak, H. Tsuchiya, J. Kunze, V. Haeublein, L. Frey, and P. Schmuki, *Nano Lett.*, **6**, 1080 (2006).
10. J. H. Park, S. Kim, and A. J. Bard, *Nano Lett.*, **6**, 24 (2006).
11. T. Umebayashi, T. Yamaki, H. Itoh, and K. Asai, *Appl. Phys. Lett.*, **81**, 454 (2002).
12. J. H. Park, O. O. Park, and S. Kim, *Appl. Phys. Lett.*, **89**, 163106 (2006).
13. P. Hoyer, *Langmuir*, **12**, 141 (1996).
14. Z. Su and W. Zhou, *Adv. Mater.*, **20**, 1 (2008).
15. J. M. Macak, H. Tsuchiya, A. Ghicov, K. Yasuda, R. Hahn, S. Bauer, and P. Schmuki, *Curr. Opin. Solid State Mater. Sci.*, **11**, 3 (2007).
16. T. Kasuga, M. Hiramatsu, A. Hoson, T. Sekino, and K. Niihara, *Langmuir*, **14**, 3160 (1998).
17. Q. Chen, W. Zhou, G. H. Du, and L.-M. Peng, *Adv. Mater.*, **14**, 1208 (2002).
18. B. D. Yao, Y. F. Chan, X. Y. Zhang, W. F. Zhang, Z. Y. Yang, and N. Wang, *Appl. Phys. Lett.*, **82**, 281 (2003).
19. M. S. Sander, M. J. Côté, W. Gu, B. M. Kile, and C. P. Tripp, *Adv. Mater.*, **16**, 2052 (2004).
20. A. Michailowski, D. AlMawlawi, G. Cheng, and M. Moskovits, *Chem. Phys. Lett.*, **349**, 1 (2001).
21. H. Imai, Y. Takei, K. Shimizu, M. Matsuda, and H. Hirashima, *J. Mater. Chem.*, **9**, 2971 (1999).
22. M. Adachi, Y. Murata, M. Harada, and S. Yoshikawa, *Chem. Lett.*, **8**, 942 (2000).
23. Yung-Huang Chang, Shun-Min Wang, Chien-Min Liu, and Chih Chen, *Journal of The Electrochemical Society*, **157**(11) K236-K241 (2010).
24. Chien-Min Liu, Chih Chen, and Hsyi-En Cheng, *Journal of The Electrochemical Society*, **158**(3) K58-K63 (2011).
25. C. J. Yang, S. M. Wang, S. W. Liang, Y. H. Chang, C. Chen, and J. M. Shieh, *Appl. Phys. Lett.*, **90**, 033104 (2007).
26. S. D. Mo and W. Y. Ching, *Phys. Rev. B*, **57**, 15219 (1998).
27. D. Routkevitch, A. N. Govyadinov, and P. P. Mardilovich, *Proceedings of the ASME Int. Mechanical Engineering Congress, MEMS*, Vol. 2, Orlando (Florida), 2000, pp. 39–44.
28. Y. Du, W. L. Cai, C. M. Mo, J. Chen, L. D. Zhang, and X. G. Zhu, *Appl. Phys. Lett.*, **74**, 2951 (1999).
29. Y. Shen, R. P. Jia, H. Q. Luo, X. G. Chen, D. S. Xue, and Z. D. Hu, *Spectrochimica Acta Part A*, **60**, 1007 (2004).
30. D. Li, N. Ohashi, S. Hishita, T. Kolodiazhnyi, and H. Haneda, *J. Solid State Chem.*, **178**, 3293 (2005).
31. D. Fang, K. Huang, S. Liu, and J. Huang, *J. Braz. Chem. Soc.*, **19**, 1059 (2008).
32. Y. Lei, L. D. Zhang, G. W. Meng, G. H. Li, X. Y. Zhang, C. H. Liang, W. Chen, and S. X. Wang, *Appl. Phys. Lett.*, **78**, 1125 (2001).
33. J. M. Wu, H. C. Shih, and W. T. Wu, *J. Vac. Sci. Technol. B*, **23**, 2122 (2005).
34. E. d. Sun, F. H. Su, Y. T. Shih, H. L. Tsai, C. H. Chen, M. K. Wu, J. R. Yang, and M. J. Chen, *Nanotechnology*, **20**, 445202 (2009).
35. Y. Li, C. W. Wang, L. R. Zhao, and W. M. Liu, *J. Phys. D: Appl. Phys.*, **42**, 045407 (2009).
36. A. Kongkanand, K. Tvrdy, K. Takechi, M. Kuno, and P. V. Kamat, *J. Am. Chem. Soc.*, **130**, 4007 (2008).
37. K. W. Liu, J. G. Ma, J. Y. Zhang, Y. M. Lu, D. Y. Jiang, B. H. Li, D. X. Zhao, Z. Z. Zhang, B. Yao, and D. Z. Shen, *Solid-State Electron.*, **51**, 757 (2007).
38. Y. Y. Lin, C. W. Chen, W. C. Yen, W. F. Su, C. H. Ku, and J. J. Wu, *Appl. Phys. Lett.*, **92**, 233301 (2008).
39. Y. H. Chang, C. M. Liu, Y. C. Tseng, C. Chen, C. C. Chen, and H. E. Cheng, *Nanotechnology*, **21**, 225602 (2010).
40. M. Dutta and D. Basak, *Appl. Phys. Lett.*, **92**, 212112 (2008).
41. I.-S. Jeong, J. H. Kim, and S. Im, *Appl. Phys. Lett.*, **83**, 2946 (2003).
42. A. M. Cowley and S. M. Sze, *J Appl. Phys.*, **36**, 3212 (1965).
43. J. W. Yoon, T. Sasaki, and N. Koshizaki, *Thin Solid Films*, **483**, 276 (2005).